Proceedings of the 16th European Turbomachinery Conference (ETC16)
Turbomachinery, Fluid Dynamics and Thermodynamics,
March 24-28, 2025; Hannover, Germany

Minimizing gas accumulation in two-phase flow within a diverging horizontal channel using cross-flow millimeter-size steps

Michael Mansour*[1,2], Nicola Zanini[3], Mena Shenouda[2], Michele Pinelli[3], Alessio Suman[3], and Dominique Thévenin[2]

[1]Mechanical Power Engineering Department, Faculty of Engineering—Mataria, Helwan University, Cairo 11718, Egypt
[2]Laboratory of Fluid Dynamics & Technical Flows, University of Magdeburg "Otto Von Guericke", 39106 Magdeburg, Germany
[3]University of Ferrara - Department of Engineering, Via Saragat 1, 44122, Ferrara, Italy

Abstract

Low-pressure separation zones in diffusers can lead to large air accumulations during two-phase flows, reducing pressure recovery. This issue is responsible for the performance drop in centrifugal pumps handling gas-liquid flows. Unlike pumps, diffusers without rotating components allow for more precise experimental characterization. This study aims to reduce gas accumulations through geometric modifications using cross-flow toothed steps. The diffuser is designed with an increasing included angle to ensure flow separation. Various two-phase flows were considered and recorded with high-speed cameras. Three toothed steps with teeth heights of 2, 5, and 8 mm were examined. The results indicate that these cross-flow steps significantly reduce gas accumulations, particularly at high water flow. Generally, the steps could enhance bubble dispersion and increase turbulence, thereby reducing gas accumulations. These findings will validate computational models and aid in optimizing real centrifugal pumps.
Keywords: Turbulent two-phase flow, Gas accumulation, Diverging channel, Diffusers, Centrifugal pumps.

1 Introduction

Gas-liquid two-phase flows are prevalent in various engineering and energy applications [1–4]. These flows present significant challenges due to their complex dynamics and unsteady interactions, even at low gas contents. Diffusers, with their variable cross-sectional areas, further complicate these flows by introducing flow separation and potential gas accumulation within the diverging section. This hinders pressure recovery. Such gas accumulations are similar to those found in centrifugal pump impeller channels under two-phase conditions, leading to flow instabilities and significantly reduced performance [5–11]. Numerical simulations of these complex flows often struggle to accurately capture the intricate turbulent interactions between the two phases at high flow rates [12–15]. Therefore, further experimental characterization is crucial.

This study is conducted within the framework of existing turbomachinery research, focusing on the critical impact of gas accumulation within diverging impeller channels on centrifugal pump performance. While these pumps function reliably with pure liquids, their efficiency significantly decreases when handling two-phase mixtures. As gas content increases, rapid accumulation, flow instabilities, and even pump "pump breakdown" can occur [4, 8, 16–20]. Therefore, reducing or preventing gas accumulation is a primary objective in research focused on improving two-phase pump performance [21].

Previous studies on two-phase flows have primarily focused on horizontal rectangular flow channels with constant cross-sections [22–25] or sudden changes in cross-section [2, 26–29]. However, gradual diverging channels have been less explored, especially for two-phase flows. The pressure recovery of a gas-liquid flow was studied in a vertical circular diffuser [30]. The two-phase pressure drop was also studied in a micro-scale horizontal, converging, or diverging rectangular channel [31]. It was found that the speed of the gas slowed down in the diverging section, causing the gas bubbles to merge, which strongly affected the flow behavior. Nonetheless, the majority of previous studies employed constant included angles (flat or non-curved diffuser) for the diverging sections [29–37]; where large flow separation and the development of big gas accumulations are less likely observed.

In previous research [13], we investigated two-phase flows in a horizontal, diverging channel with a gradually increasing included angle. We observed key parameters leading to gas accumulation and phase segregation. Large recirculation zones resulting from flow separation trapped bubbles, causing significant accumulations. Increasing air flow rate monotonically increased accumulation size. However, increasing the water flow rate initially expanded accumulation size due to larger recirculation zones but then decreased it due to strong turbulence fluctuations. Surprisingly, even at low gas contents (0.05% by volume), a large air pocket formed near the end of the diverging section, impacting velocity distribution and reducing pressure recovery. Our findings identified factors contributing to decreasing gas accumulation, such as reducing flow separation or increasing turbulence [13].

Previous research [14, 38, 39] have also compared experimental data from [13] with various numerical models to improve prediction accuracy. The Reynolds stress model (RSM) combined with the volume of fluid (VOF) method showed promising results in predicting gas accumulation size and shape [14]. However, numerical errors increased at high Reynolds numbers. The disperse two-fluid approach

*Corresponding author: m.botros@m-eng.helwan.edu.eg, michael.mansour@ovgu.de

and turbulence modeling struggled to detect gas accumulation in some cases [38]. The most accurate predictions were achieved using a hybrid multiphase approach combining Eulerian-Eulerian solvers, VOF enhancements, and large eddy simulations (LES) [39]. This approach effectively captured flow characteristics and predicted gas accumulation size and position. However, its accuracy depended on the specified bubble size, highlighting the need for further development of computational methods, including bubble size distribution. The limitations of numerical studies in predicting gas accumulation in diverging channels emphasize the continued importance of experimental investigations.

Accordingly, to minimize gas accumulation in two-phase flows within diverging channels, this study employs upstream cross-flow millimeter-size steps made of thin metal sheets. These steps should ideally reduce the gas accumulation by 1) enhancing turbulence, 2) breaking larger bubbles into finer ones, and 3) promoting vertical bubble dispersion while 4) minimizing additional flow separation on the upper diffuser side. These flow mechanisms, i.e., turbulence enhancement, bubble size reduction, vertical redistribution, and flow separation control, are integral to achieving the intended reduction of gas accumulation. Three toothed metal sheets with varying tooth heights (2 mm, 5 mm, 8 mm) were investigated. The same experimental setup and diffuser geometry used in previous research [13, 14, 38, 39] was utilized. To ensure flow separation, the diffuser was designed with an increasing included angle. A wide range of two-phase flow conditions (Re_L =59,530–78,330, Re_G =3–9.25) were considered, with two-phase interactions recorded using high-speed cameras. Results show a clear reduction in gas accumulations for some flow conditions. This research provides a validation database for predictive models, enabling improved accuracy in numerical simulations for two-phase flows. Unlike pumps, the simplified diffuser configuration used in this study ensures a more accurate and detailed experimental characterization, which facilitates the validation and refinement of existing models. Furthermore, the findings will contribute to design guidelines for optimizing centrifugal pumps by offering insights into minimizing gas accumulation within the impeller channels.

2 Experimental set-up

A sketch of the experimental set-up is shown in Figure 1. To allow for clear observation of the flow and optical measurements, the test section of the diverging part was manufactured from transparent acrylic glass. As shown, a submersible pump circulates water from a 6.0 m^3 water tank through the test section. Air from a compressed air supply is mixed with the water flow at a mixing point before entering the channel. The air flow is inserted into the mixing joint through 21 tiny holes, each 1.0 mm in diameter, which are arranged around the circumference of the mixing joint. The flow rates of water and air are independently measured and regulated using control valves. The water flow is measured with an electromagnetic flow meter (Endress+Hauser Promag 30F with an accuracy of $\pm$ 0.5% RD), while air flow is controlled by a rotameter (Yokogawa RGC1263 with $\pm$ 2.5% RD accuracy). The temperature of both water and air is measured separately before being mixed, using two RTD (Resistance Temperature Detector) temperature sensors (Pt100 Sensor Probe, Class B with a maximum absolute error of $\pm$ 0.3 K). For accurate control of the air flow, the air supply includes a service unit, a control valve, a pressure regulator, and a restriction valve. As shown in Figure 1, the pressure changes along the diverging section are monitored by eight pressure sensors (Cerabar T PMC131 ($-1:+1$ bar) with $\pm$ 0.5% RD accuracy). The average uncertainty associated with the reported pressure measurements is estimated to be approximately 2.9%. Further information about the measurement devices and their accuracy can be found in [13].

The channel has upstream and downstream rectangular cross-sections of 40 x 44 mm and 100 x 44 mm, respectively. This results in a hydraulic diameter ratio of 1.45, where the upstream and downstream hydraulic diameters are $d_{hu} = 42$ mm and $d_{hd} = 61$ mm, respectively. The upstream channel has enough length before the diffuser to establish fully-developed flow conditions. The lengths of the straight upstream and downstream parts are $L_1 = 34d_{hu}$ and $L_2 = 15.5d_{hu}$, respectively. The diffuser is designed with a gradually increasing included angle along the flow direction. In this way, the flow separates within wide flow conditions, forming large recirculation zones, and consequently, air accumulation. Explicitly, the diffuser begins with a half-included angle of 6° whose upper curve is described by the function $x = 13.5y - y^2/10 - 230$ (x: axial direction, y: vertical direction). Accordingly, the half-included angle increases gradually to 16°. The flow channel is positioned horizontally because, in this configuration, the gravitational force acts perpendicular to the flow direction. This setup, while not identical to the Coriolis force in pumps, provides a degree of similarity in terms of lateral force interactions, which would not be achievable in a vertical channel where gravity acts parallel to the flow direction. Moreover, the horizontal orientation effectively replicates gas accumulation phenomena analogous to those observed in impeller channels. This approach allows for a meaningful exploration of gas accumulation reduction techniques, that can be later applied in centrifugal pumps.

The single-phase flow (pure water) velocities were recorded for the top part of the diffuser using a two-component Laser Doppler Anemometry (LDA) system (Dantec Dynamics 2-D). The total estimated uncertainty in the velocity measurements is quantified to be less than 0.5%. Utilizing an automatic traversing system, the velocity was measured for a grid of 325 measurement points at the mid-longitudinal section of the channel as shown in Figure 2a, and then the velocity field was deduced. The horizontal and vertical grid spaces are x = 10 mm and y = 7.5 mm. At each measurement point, a total of 25,000 samples were collected to ensure high statistical reliability. The average data acquisition rate is about 1.5 kHz. The precise location of each measurement point was determined through calibration, accounting for the refraction of laser beams as they passed through the acrylic glass and water. Further details about the LDA system and the calibration based on the refraction indices can be found in [40]. Glass spheres with a mean diameter of 10 µm and a density of 1000 kg/m^3 were employed as tracer particles for LDA measure-

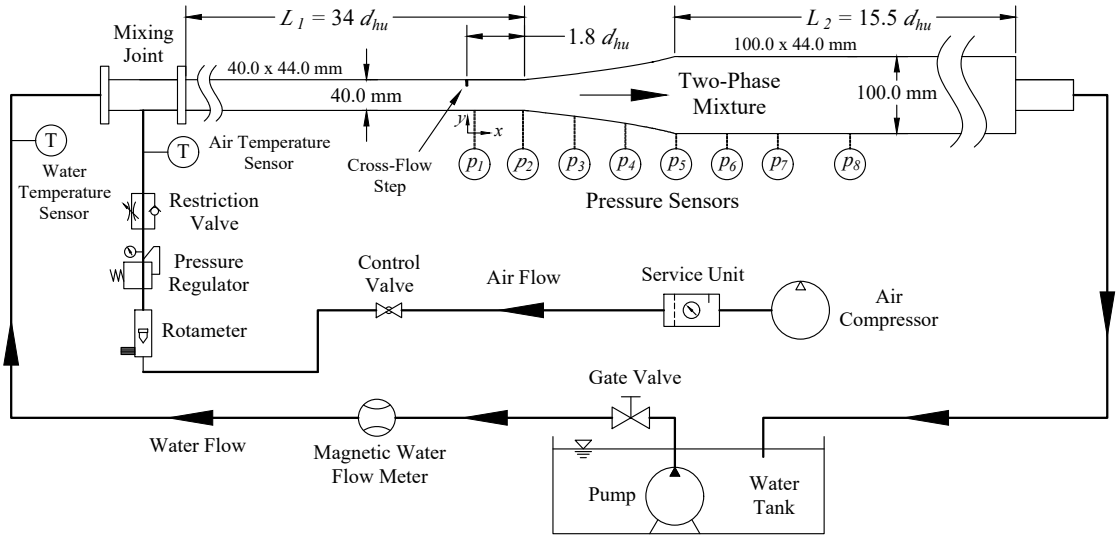

Figure 1: Sketch of the experimental loop.

ments. To record the size of the accumulated gas, shadowgraphy images were captured using a high-speed camera. The test section was illuminated from behind by two LED (Light Emitting Diode) panels (facing the cameras), as depicted in Figure 2b. This arrangement produced dark outlines of the water-air interface, allowing for clear visualization of accumulated gas. Similarly, the bubble size distributions (BSD) have been recorded within a sample window (length = 25 mm and height = 40 mm) just before the beginning of the diffuser using another high-speed camera as shown in Figure 2c. The calculated uncertainty of the measured bubble diameters yields a root mean square value of less than 4.9%. The BSD measurement is substantial for validating numerical models since it can strongly affect the prediction accuracy [39].

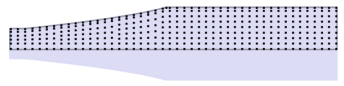

(a) Grid points of LDA

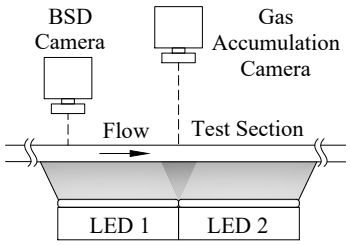

(b) Shadowgraphy top view

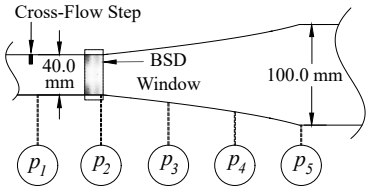

(c) BSD window

Figure 2: Details of the measurements

Three different toothed cross-flow steps with varying teeth heights of 2 mm, 5 mm, and 8 mm were studied as shown in Figure 3. These metal sheets have a thickness of 0.5 mm and were always installed at a distance of 1.8 d_{hu} before the diverging part with the teeth on the top side of the channel as presented in Figure 3a. The reference cross-sectional area of the channel without steps (0 mm) is shown in Figure 3b, while the other subfigures show the dimensions of the three cross-flow steps. Here, only the tooth height was modified; all other dimensions remained constant.

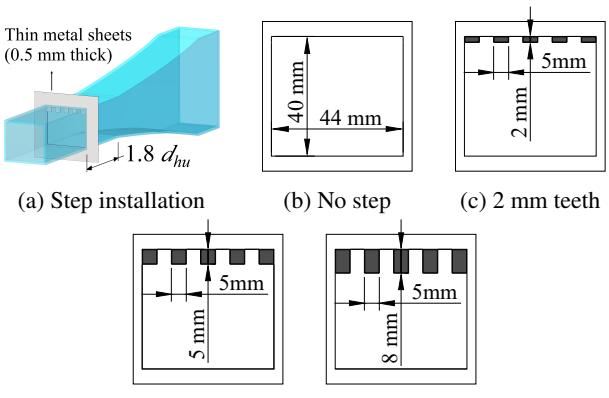

(a) Step installation (b) No step (c) 2 mm teeth

(d) 5 mm teeth (e) 8 mm teeth

Figure 3: Details of the cross-flow steps studied.

3 Results

Based on the results of the previous investigations [13, 14, 38–40], different flow conditions were selected for the present investigations. Two different single-phase flow conditions of water (Q_L) were considered. Further, two different air flow rates (Q_G) were chosen, resulting in a total of 4 different two-phase cases. Accordingly, different sizes and shapes of gas accumulations are covered to investigate the effects of cross-flow steps in detail. Table 1 lists the considered flow conditions. The superficial Reynolds numbers of water (Re_L) and air (Re_G) are calculated by Equation 1. The superficial Reynolds number is a dimensionless parameter that charac-

terizes the flow behavior of each phase as if it were flowing alone through the entire cross-sectional area of the channel. In Equation 1, ρ is the density, u is the superficial velocity in the inlet channel, calculated by Equation 2, μ is the dynamic viscosity, the subscripts L and G refer to water and air, respectively, A_u is the upstream cross-sectional area of the channel, and $\dot{\varepsilon}$ is the gas volume fraction, determined by Equation 3. Please note that the setup was designed to operate under non-cavitating flow conditions to eliminate the potential confusion between vapor and air bubbles. To confirm cavitation-free conditions, the minimum cavitation number was calculated ($\sigma = 18.5$) and found to be significantly higher than the critical value ($\sigma_{crit} = 0.3$), even under the maximum velocity, considering the flow fluctuations and the largest tooth height. Accordingly, no cavitation phenomena were observed during the entire experiments.

$$\mathrm{Re}_{L,G} = \frac{\rho_{L,G}\, u_{L,G}\, d_{hu}}{\mu_{L,G}} \tag{1}$$

$$u_{L,G} = \frac{Q_{L,G}}{A_u} \tag{2}$$

$$\dot{\varepsilon} = \frac{Q_G}{Q_G + Q_L} \tag{3}$$

Table 1: Details of the considered flow conditions.

Case#	Q_L (m^3/h)	Q_G (L/h)	Re_L	Re_G	$\dot{\varepsilon}$ (%)
1	9.5	0	59530	0	0
2	12.5	0	78330	0	0
3	9.5	7.07	59530	3.10	0.074
4	9.5	21.21	59530	9.25	0.223
5	12.5	7.07	78330	3.10	0.056
6	12.5	21.21	78330	9.25	0.169

Measurements of single-phase velocities

Although the flow in the channel is inherently three-dimensional [14], the velocity measurements were primarily conducted at the midsection. This region effectively captures key phenomena, including jet direction, flow separation, and turbulence intensity, all of which influence gas accumulation behavior under two-phase conditions. The data obtained at the midsection is sufficient for assessing the flow structure and enables meaningful comparisons between the various cases studied. Figure 4 shows the measured single-phase velocity magnitude and the velocity fluctuations for all considered configurations. As shown, a flow separation occurs on the upper part of the diffuser in all cases. In the reference case (without steps), the flow separation is slightly smaller compared to the cases with cross-flow steps. Additionally, it becomes undesirably larger as the teeth height increases for both flow rates. Further, the maximum values of velocity fluctuations of the 2-mm teeth decrease when compared to those of the reference case. However, for the 5-mm and 8-mm teeth, much higher velocity fluctuations are observed on the upper surface of the diffuser. The maximum values of velocity fluctuations of the 8 mm teeth exceed those of the reference case. These two effects would be useful to reduce the gas accumulation under two-phase conditions.

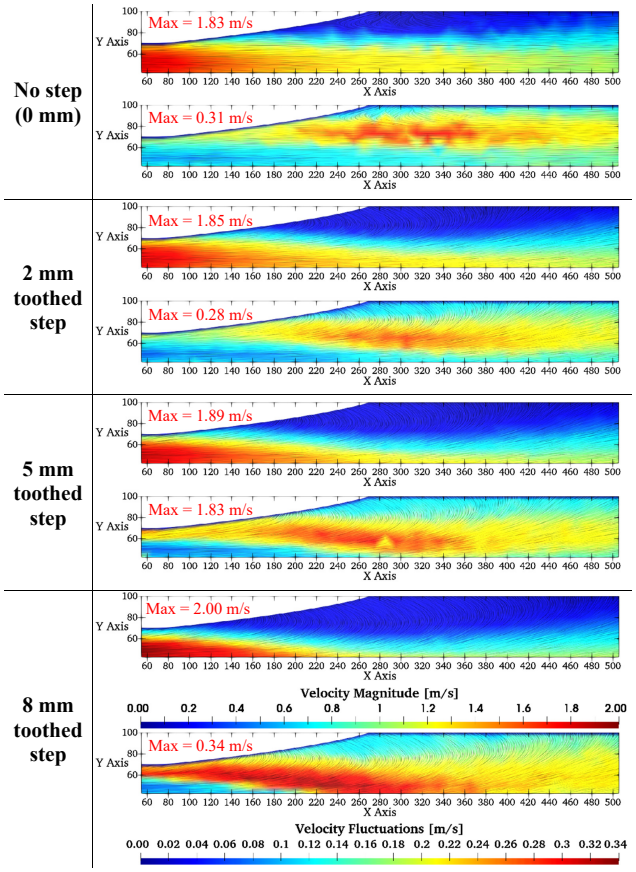

(a) **Case 1** ($\mathrm{Re}_L = 59{,}530$, $\mathrm{Re}_G = 3.1$)

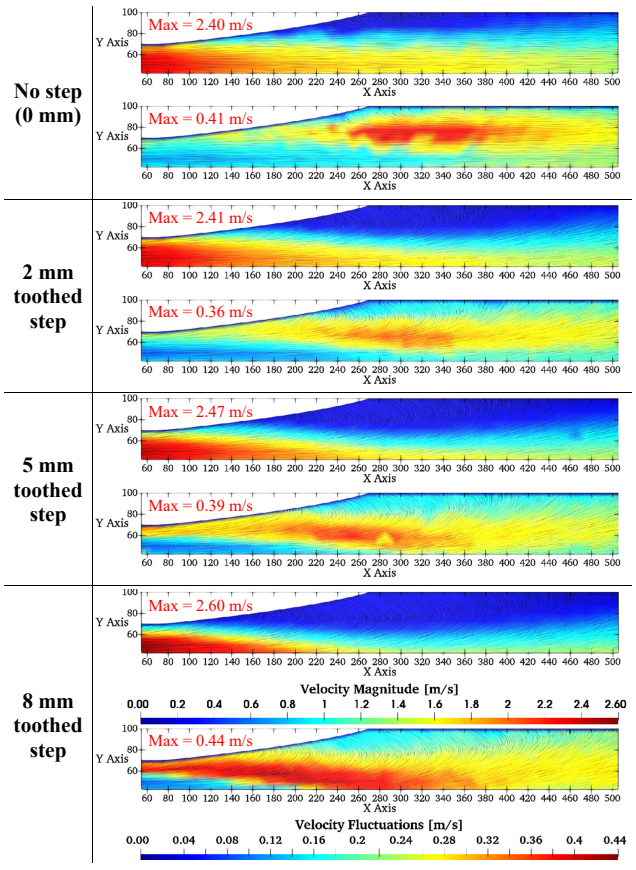

(b) **Case 2** ($\mathrm{Re}_L = 59{,}530$, $\mathrm{Re}_G = 9.25$)

Figure 4: Single-phase velocity measurements.

Measurements of two-phase flow conditions

The bubble dispersion and size distributions at the inlet were measured and compared. As shown in Figure 5 for the reference case, large bubbles are present on the top surface for all four two-phase conditions (Cases 3 to 6). Bubbles are notably larger in Case 4 with low water and high air flow. For the 2 mm teeth, a stratified flow develops at low flow (Cases 3 and 4) behind the step, where the teeth are too short to disturb the bubbles. The step merely slows down bubbles near the inlet, leading to bubble coalescence and increased gas accumulation. However, this does not occur at higher water flow rates (Cases 5 and 6), where bubble dispersion improves slightly. For the 5 mm toothed step, bubble dispersion is observed across all flow conditions, with further improvement in the vertical direction for the 8 mm step, where finer bubbles are also seen. Crushing larger bubbles into finer ones and pushing them toward the channel center typically reduces accumulated gas in the separation zone at the top of the diverging part.

Figure 6 shows the measured BSD for different geometries in a sample two-phase flow (Case 5). The median diameter (D_{median}), the Sauter mean diameter D_{32}, and the standard deviation (σ) of each distribution are also shown. Here, the median diameter is the size at which half of the bubbles in a distribution are larger and half are smaller. The Sauter mean diameter is the ratio of the total volume to the total surface area of the bubbles, representing a measure of the average bubble size. The median diameter (D_{median}) across all cases is around 0.5 mm. However, the Sauter mean diameter (D_{32}) and standard deviation (σ) decrease with increasing teeth height, confirming effective bubble breakup by the cross-flow steps.

For the reference case (without steps), the four selected two-phase cases lead to large gas accumulations with remarkable changes in size and shape, as can be seen in Figure 7. Here, the largest accumulation is seen for Case 4, as it has a low water flow and a high gas flow, while the smallest accumulation occurs for Case 5, which has a high water flow and a low gas flow. For the 2 mm toothed step, the gas accumulation becomes slightly larger for most cases (Cases 3, 4, and 5) because this small step cannot disperse the bubbles, rather it decelerates them near the channel inlet (see again Figure 5). Accordingly, the gas accumulation is undesirably larger.

In the experiments, the accumulated air consistently fills the entire width of the channel, with only instantaneous unsteady variations observed locally at the beginning of the accumulation. To determine the average size of the accumulated gas, a grayscale average image was generated from 1500 instantaneous images captured at a low frequency of 50 Hz, providing a stable representation of the air-water interface. This effectively eliminates all transient and unsteady effects in the interface and also ensures that any potential three-dimensional variations are negligible in the observed results. These averaged images were then binarized using an intensity threshold (I) determined from their brightness spectra. Figure 8 presents representative examples of the averaged and binarized images. A MATLAB script was employed to identify the black pixels corresponding to the accumulated air boundary. The script then located the middle pixel of this boundary to define the bottom edge of the accumulated gas. The calculated mean boundaries, as determined by the script, are overlaid on the binarized images in Figure 8 as thin white lines. For a detailed description of the calculations, please refer to [13, 40].

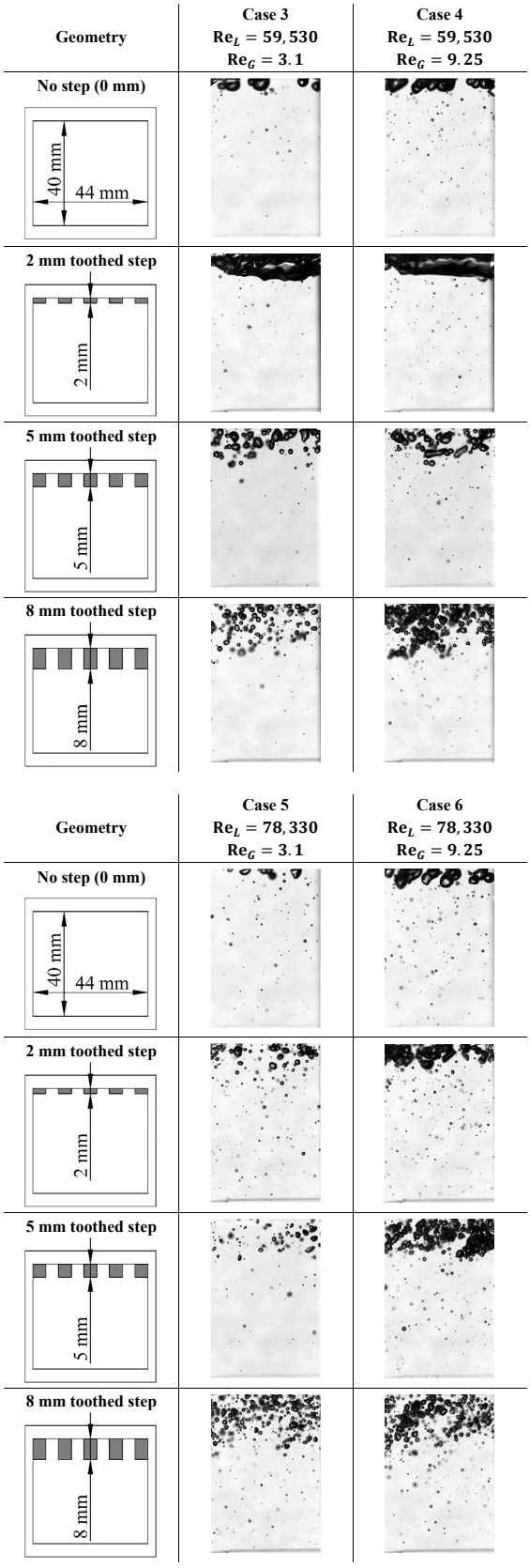

Figure 5: Bubble dispersion for all two-phase configurations just before the diffuser inlet (Camera focus is set on the mid-longitudinal section).

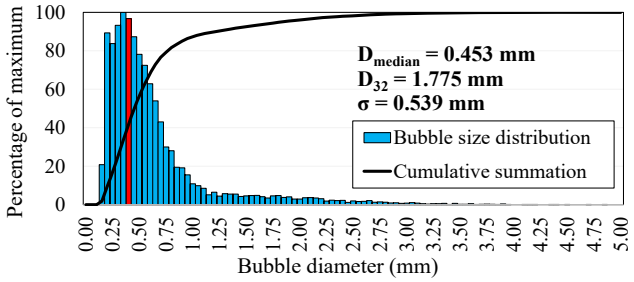

(a) Reference case (without steps)

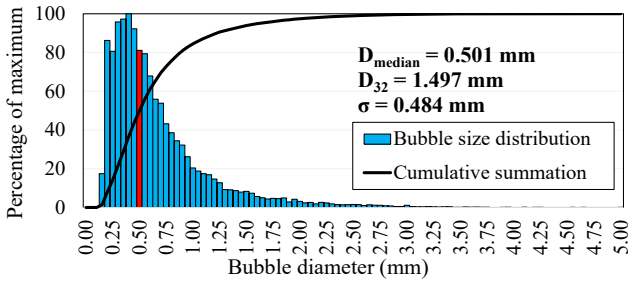

(b) 2 mm teeth

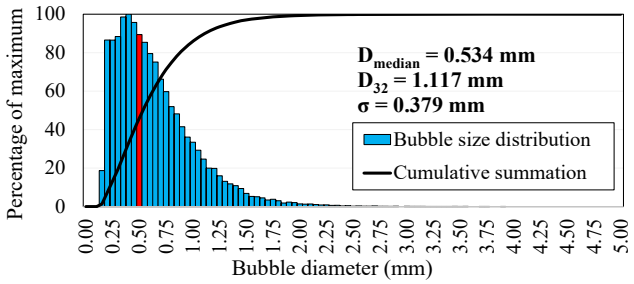

(c) 5 mm teeth

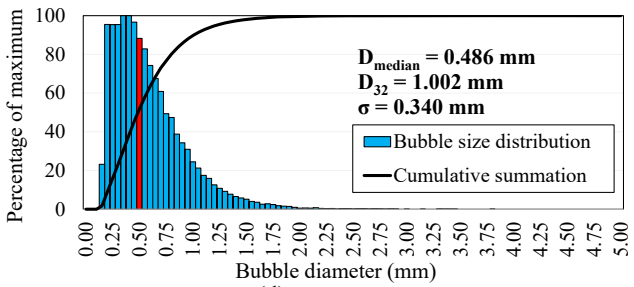

(d) 8 mm teeth

Figure 6: Bubble size distributions (BSD) of different geometrical conditions for Case 5.

Figure 9 presents the gas void fraction of the accumulated gas in the channel for all studied cases. This fraction is calculated by dividing the average accumulated gas volume by the total channel volume, measured from the inlet plane of the diverging section. As anticipated, the 2 mm toothed step generally leads to greater gas accumulation compared to cases without steps. Nevertheless, a gradual decrease in accumulated gas is observed as the tooth height increases to 5 mm and 8 mm. Notably, these larger cross-flow steps prove more effective in reducing gas accumulation under high flow conditions (Cases 5 and 6), as illustrated in Figure 9. For instance, the 8 mm toothed step could reduce the size of the accumulated gas by approximately 14%, 8%, 68%, and 72% for Cases 3, 4, 5, and 6, respectively.

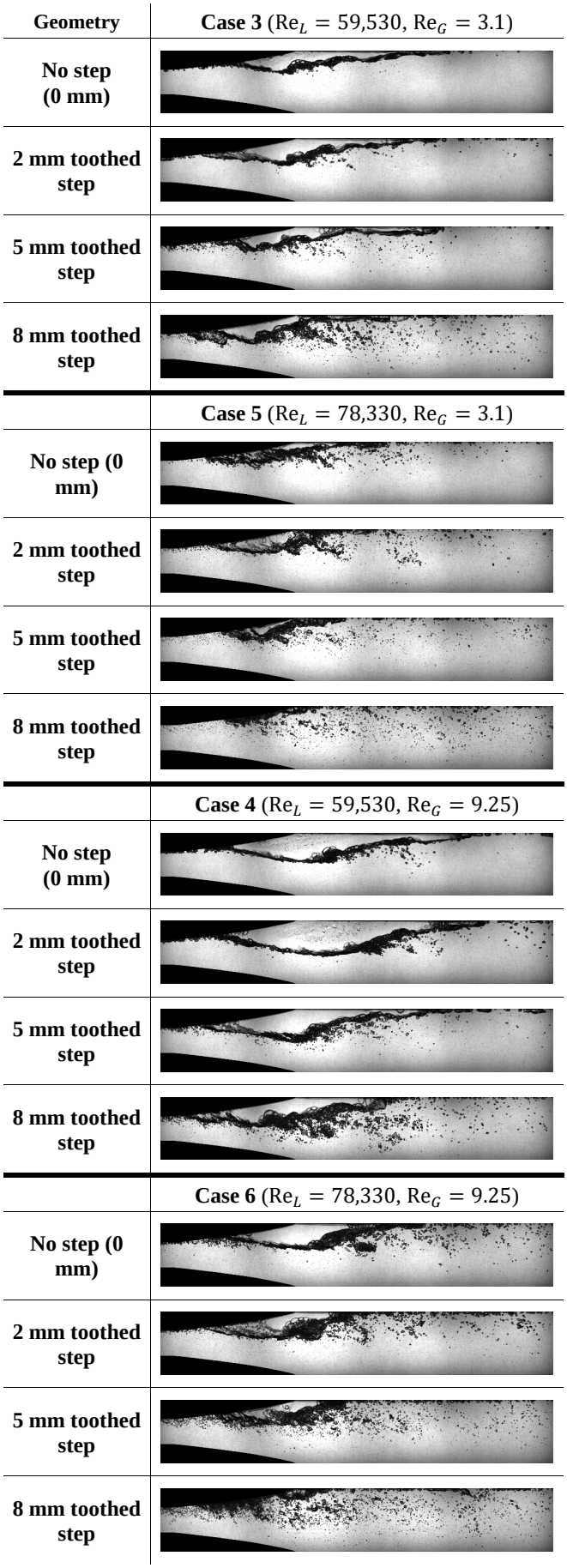

Figure 7: Gas accumulations for all two-phase configurations.

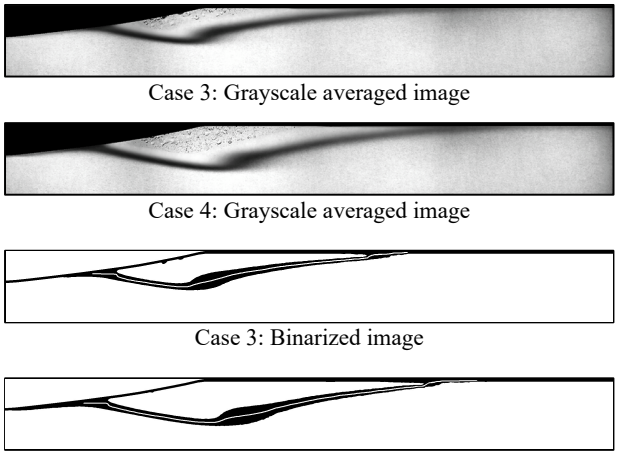

Figure 8: Illustration of the image processing for quantifying the accumulated gas.

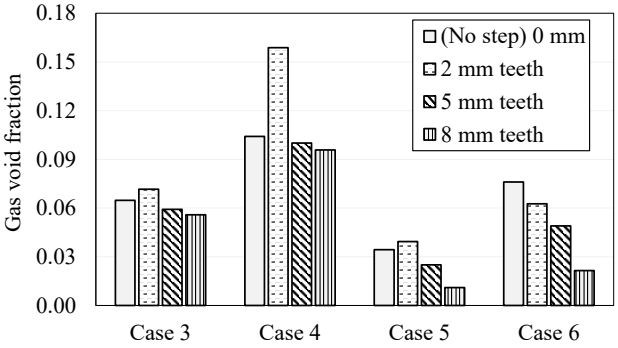

Figure 9: Gas void fraction for all considered cases.

Pressure recovery

Figure 10 illustrates the impact of accumulated gas on pressure recovery within the diffuser. Pressure measurements were taken at eight distinct axial locations along the streamwise direction (refer back to Figure 1). Due to the highly turbulent nature of the flow, an average value of the pressure was calculated after continuously monitoring the readings at each point for several minutes at a frequency of 8 Hz. Pressure sensor number 2, installed at the diffuser inlet (i.e., at $x = 0$), was used as a reference point for the pressure difference. The values shown are then normalized by the maximum pressure difference of the single-phase flow of each case ($p_8 - p_2$). The pressure results are shown in Figure 10 for Re_L = 59,530 and Re_L = 78,330. As can be seen for the reference configuration, a reduction in the pressure recovery is taking place as the gas accumulation size increases. No significant improvement in the pressure recovery within the diffuser could be seen for the 2 mm case since these short teeth fail to reduce gas accumulation. For the 5 mm teeth, the improvements are limited due to the increased flow separation. Nonetheless, a significant improvement can be seen in the pressure recovery of the 8 mm teeth at Re_L = 78,330 regardless of the increased separation since it could highly reduce the gas accumulations. Here, the two-phase pressure recovery is very similar to that of single-phase flow.

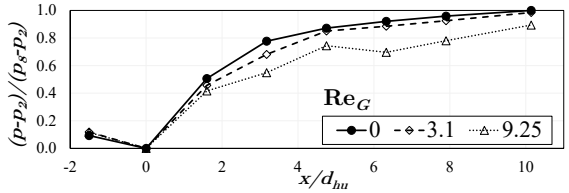

(a) **Rerence case (no step), $\mathrm{Re}_L = 59{,}530$**

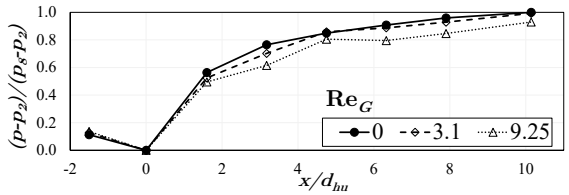

(b) **Rerence case (no step), $\mathrm{Re}_L = 78{,}330$**

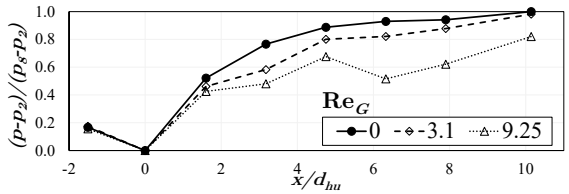

(c) **2 mm teeth, $\mathrm{Re}_L = 59{,}530$**

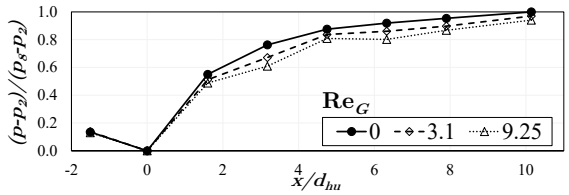

(d) **2 mm teeth, $\mathrm{Re}_L = 78{,}330$**

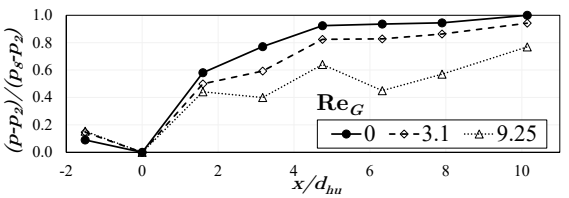

(e) **5 mm teeth, $\mathrm{Re}_L = 59{,}530$**

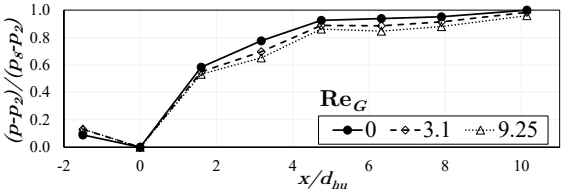

(f) **5 mm teeth, $\mathrm{Re}_L = 78{,}330$**

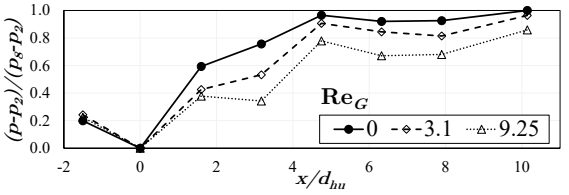

(g) **8 mm teeth, $\mathrm{Re}_L = 59{,}530$**

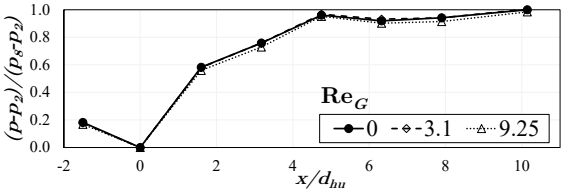

(h) **8 mm teeth, $\mathrm{Re}_L = 78{,}330$**

Figure 10: Pressure recovery for all considered cases.

4 Conclusions

Various gas-liquid two-phase conditions were experimentally investigated in a horizontal diffuser, where big gas accumulations develop due to flow separation. The velocity measurements indicated large separation zones on the upper side of the diffuser, where air accumulates. To reduce the size of the accumulated gas, three upstream cross-flow toothed steps with teeth heights of 2, 5, and 8 mm were used. The separation increases with increasing the height of the teeth. However, the turbulence fluctuations are also favorably improved. The two-phase interactions and the bubble size distributions were recorded by shadowgraphy utilizing high-speed cameras. The results indicate that the 2 mm toothed step is not effective in dispersing the bubbles or reducing the accumulated gas since the teeth are too short. Nonetheless, the 5- and 8-mm steps produce much stronger bubble dispersion and break-up, leading to significantly reduced gas accumulations. These effects are more pronounced at high water flows. Additionally, the 8 mm step revealed improved pressure recovery at high water flows with almost no decay under two-phase conditions. These experimental results will be used in the validation of numerical simulations and help improve the design of actual centrifugal pumps.

Acknowledgements

This work is part of a project funded by VDMA (Verband Deutscher Maschinen- und Anlagenbau) and BMWi (Bundesministeriums für Wirtschaft und Energie) under number IGF 23051.

Nomenclature

A_u	upstream cross-sectional area [m^2]
D_{32}	Sauter mean diameter [mm]
D_{median}	median diameter [mm]
d_{hd}	downstream hydraulic diameter [m]
d_{hu}	upstream hydraulic diameter [m]
I	Light intensity [cd]
L_1	upstream straight pipe length [m]
L_2	downstream straight pipe length [m]
P_2	reference pressure (sensor 2) [mbar]
p	local pressure [mbar]
Q_G	gas volume flow rate [L/h]
Q_L	liquid volume flow rate [m^3/s]
Re_G	superficial gas Reynolds number
Re_L	superficial liquid Reynolds number
u_G	superficial gas velocity [m/s]
u_L	superficial liquid velocity [m/s]
x	axial distance [m]
y	vertical distance [m]

Greek symbols

$\dot{\varepsilon}$	gas volume fraction [%]
ρ_G	density of gas [kg/m^3]
ρ_L	density of liquid [kg/m^3]
σ	standard deviation of BSD [mm]
μ_G	viscosity of gas [Pa s]
μ_L	viscosity of liquid [Pa s]

Subscripts

d	downstream
G	gas
h	hydraulic
L	liquid
u	upstream

Acronyms

% RD	Percentage of reading (for accuracy quantification)
BSD	Bubble Size Distribution
LDA	Laser Doppler Anemometry
LED	Light Emitting Diode
LES	Large Eddy Simulation
RSM	Reynolds Stress Model
RTD	Resistance Temperature Detector
VOF	Volume Of Fluid

References

[1] M. E. Ewing, J. J. Weinandy, and R. N. Christensen. "Observations of Two-Phase Flow Patterns in a Horizontal Circular Channel". In: *Heat Transf. Eng.* 20.1 (Feb. 1999), pp. 9–14. ISSN: 0145-7632. DOI: 10.1080/014576399271682.

[2] I. Y. Chen, C.-Y. Tseng, Y.-T. Lin, and C.-C. Wang. "Two-phase flow pressure change subject to sudden contraction in small rectangular channels". In: *Int. J. Multiph. Flow* 35.3 (Mar. 2009), pp. 297–306. ISSN: 03019322. DOI: 10.1016/j.ijmultiphaseflow.2008.10.008.

[3] A. Sharma, V. Tyagi, C. Chen, and D. Buddhi. "Review on thermal energy storage with phase change materials and applications". In: *Renew. Sustain. Energy Rev.* 13.2 (Feb. 2009), pp. 318–345. ISSN: 13640321. DOI: 10.1016/j.rser.2007.10.005.

[4] M. Mansour, B. Wunderlich, and D. Thévenin. "Effect of tip clearance gap and inducer on the transport of two-phase air-water flows by centrifugal pumps". In: *Exp. Therm. Fluid Sci.* 99 (2018), pp. 487–509. DOI: 10.1016/j.expthermflusci.2018.08.018.

[5] J. J. Manzano Ruiz. "Experimental and theoretical study of two-phase flow in centrifugal pumps". PhD thesis. Massachusetts Institute of Technology, 1980.

[6] Z. Zhu, P. Xie, G. Ou, B. Cui, and Y. Li. "Design and Experimental Analyses of Small-flow High-head centrifugal-vortex Pump for Gas-Liquid Two-phase Mixture". In: *Chinese J. Chem. Eng.* 16.4 (Jan. 2008), pp. 528–534. ISSN: 10049541. DOI: 10.1016/S1004-9541(08)60116-0.

[7] L. Barrios and M. G. Prado. "Experimental Visualization of Two-Phase Flow Inside an Electrical Submersible Pump Stage". In: *J. Energy Resour. Technol.* 133.4 (2011), p. 042901. ISSN: 01950738. DOI: 10.1115/1.4004966.

[8] M. Mansour, B. Wunderlich, and D. Thévenin. "Experimental study of two-phase air/water flows in a centrifugal pump working with a closed or a semi-open impeller". In: *ASME Turbo Expo 2018: Turbomachinery Technical Conference and Exposition, Oslo, Norway*. 2018, V009T27A012. DOI: 10.1115/GT2018-75380.

[9] M. Mansour, S. Kopparthy, and D. Thevenin. "Investigations on the effect of rotational speed on the transport of air-water two-phase flows by centrifugal pumps". In: *Int. J. Heat Fluid Flow* 94 (2022), p. 108939. DOI: 10.1016/j.ijheatfluidflow.2022.108939.

[10] M. Hundshagen and R. Skoda. "State of the art on two-phase non-miscible liquid/gas flow transport analysis in radial centrifugal pumps Part C: CFD approaches with emphasis on improved models". In: *Int. J. Turbomach. Propuls. Power* 8.2 (2023), p. 15. DOI: 10.3390/ijtpp8020015.

[11] M. Mansour and D. Thévenin. "State of the art on two-phase non-miscible liquid/gas flow transport analysis in radial centrifugal pumps Part B: Review of experimental investigations". In: *Int. J. Turbomach. Propuls. Power* 8.4 (2023), p. 42. DOI: 10.3390/ijtpp8040042.

[12] T. Müller, P. Limbach, and R. Skoda. "Numerical 3D RANS simulation of gas-liquid flow in a centrifugal pump with an Euler-Euler two-phase model and a dispersed phase distribution". In: *11th Eur. Conf. Turbomach. Fluid Dyn. Thermodyn.* Madrid, 2015.

[13] M. Mansour, P. Kováts, B. Wunderlich, and D. Thévenin. "Experimental investigations of a two-phase gas/liquid flow in a diverging horizontal channel". In: *Exp. Therm. Fluid Sci.* 93 (2018), pp. 210–217. ISSN: 0894-1777. DOI: 10.1016/j.expthermflusci.2017.12.033.

[14] S. Kopparthy, M. Mansour, G. Janiga, and D. Thévenin. "Numerical investigations of turbulent single-phase and two-phase flows in a diffuser". In: *Int. J. Multiph. Flow* 130 (2020), p. 103333. ISSN: 0301-9322. DOI: 10.1016/j.ijmultiphaseflow.2020.103333.

[15] M. Hundshagen, M. Mansour, D. Thévenin, and R. Skoda. "Numerical investigation of two-phase air-water flow in a centrifugal pump with closed or semi-open impeller". In: *Proceedings of 13th European Turbomachinery Conference on Turbomachinery Fluid Dynamics and Thermodynamics, ETC 2019*. 2019. DOI: 10.29008/ETC2019-011.

[16] A. Poullikkas. "Effects of two-phase liquid–gas flow on the performance of nuclear reactor cooling pumps". In: *Prog. Nucl. Energy* 42.1 (Jan. 2003), pp. 3–10. ISSN: 01491970. DOI: 10.1016/S0149-1970(03)80002-1.

[17] J. Caridad, M. Asuaje, F. Kenyery, A. Tremante, and O. Aguillón. "Characterization of a centrifugal pump impeller under two-phase flow conditions". In: *J. Pet. Sci. Eng.* 63.1-4 (Dec. 2008), pp. 18–22. ISSN: 09204105. DOI: 10.1016/j.petrol.2008.06.005.

[18] A. Amoresano, G. Langella, V. Niola, and G. Quaremba. "Advanced Image Analysis of Two-Phase Flow inside a Centrifugal Pump". In: *Adv. Mech. Eng.* 6 (Jan. 2014). ISSN: 1687-8140. DOI: 10.1155/2014/958320.

[19] J. Zhu, X. Guo, F. Liang, and H.-Q. Zhang. "Experimental study and mechanistic modeling of pressure surging in electrical submersible pump". In: *J. Nat. Gas Sci. Eng.* 45 (2017), pp. 625–636. ISSN: 1875-5100. DOI: 10.1016/j.jngse.2017.06.027.

[20] W. Monte Verde, J. L. Biazussi, N. A. Sassim, and A. C. Bannwart. "Experimental study of gas-liquid two-phase flow patterns within centrifugal pumps impellers". In: *Exp. Therm. Fluid Sci.* 85 (July 2017), pp. 37–51. ISSN: 08941777. DOI: 10.1016/j.expthermflusci.2017.02.019.

[21] M. Mansour, S. B. Kopparthy, and D. Thévenin. "Improving air-water two-phase flow pumping in centrifugal pumps using novel grooved front shrouds". In: *Chem. Eng. Res. Des.* 197 (2023), pp. 173–191. ISSN: 0263-8762. DOI: 10.1016/j.cherd.2023.07.019.

[22] I. Y. Chen, Y. M. Chen, B.-C. Yang, and C.-C. Wang. "Two-phase flow pattern and frictional performance across small rectangular channels". In: *Appl. Therm. Eng.* 29.7 (May 2009), pp. 1309–1318. ISSN: 13594311. DOI: 10.1016/j.applthermaleng.2008.08.019.

[23] M. Wambsganss, J. Jendrzejczyk, D. France, and N. Obot. “Frictional pressure gradients in two-phase flow in a small horizontal rectangular channel”. In: *Exp. Therm. Fluid Sci.* 5.1 (Jan. 1992), pp. 40–56. ISSN: 08941777. DOI: 10.1016/0894-1777(92)90055-A.

[24] C. Vallée, T. Höhne, H.-M. Prasser, and T. Sühnel. “Experimental investigation and CFD simulation of horizontal stratified two-phase flow phenomena”. In: *Nucl. Eng. Des.* 238.3 (Mar. 2008), pp. 637–646. ISSN: 00295493. DOI: 10.1016/j.nucengdes.2007.02.051.

[25] W. Aziz, S. Chaturvedi, and A. Kheireddine. “Thermodynamic analysis of two-component, two-phase flow in solar collectors with application to a direct-expansion solar-assisted heat pump”. In: *Energy* 24.3 (Mar. 1999), pp. 247–259. ISSN: 03605442. DOI: 10.1016/S0360-5442(98)00089-9.

[26] I. Y. Chen, C.-C. Liu, K.-H. Chien, and C.-C. Wang. “Two-phase flow characteristics across sudden expansion in small rectangular channels”. In: *Exp. Therm. Fluid Sci.* 32.2 (Nov. 2007), pp. 696–706. ISSN: 08941777. DOI: 10.1016/j.expthermflusci.2007.09.001.

[27] F. F. Abdelall, G. Hahn, S. M. Ghiaasiaan, S. I. Abdel-Khalik, S. S. Jeter, M. Yoda, and D. L. Sadowski. “Pressure drop caused by abrupt flow area changes in small channels”. In: *Exp. Therm. Fluid Sci.* 29.4 (2005), pp. 425–434. ISSN: 0894-1777. DOI: 10.1016/j.expthermflusci.2004.05.001.

[28] W. H. Ahmed, C. Y. Ching, and M. Shoukri. “Development of two-phase flow downstream of a horizontal sudden expansion”. In: *Int. J. Heat Fluid Flow* 29.1 (Feb. 2008), pp. 194–206. ISSN: 0142727X. DOI: 10.1016/j.ijheatfluidflow.2007.06.003.

[29] M. A. Pakhomov and V. I. Terekhov. “Modeling of turbulent heat-transfer augmentation in gas-droplet nonboiling flow in diverging and converging axisymmetric ducts with sudden expansion”. In: *Energies* 15.16 (2022). ISSN: 1996-1073. DOI: 10.3390/en15165861.

[30] S. Anupriya and S. Jayanti. “Experimental and modelling studies of gas–liquid vertical annular flow through a diverging section”. In: *Int. J. Multiph. Flow* 67 (Dec. 2014), pp. 180–190. ISSN: 03019322. DOI: 10.1016/j.ijmultiphaseflow.2014.05.009.

[31] J. J. Hwang, F. G. Tseng, and C. Pan. “Ethanol-CO_2 two-phase flow in diverging and converging microchannels”. In: *Int. J. Multiph. flow* 31.5 (2005), pp. 548–570. ISSN: 0301-9322. DOI: 10.1016/j.ijmultiphaseflow.2005.01.011.

[32] E. Deniz and N. Eskin. “Hydrodynamic characteristics of two-phase flow through horizontal pipe having smooth expansion”. In: *ISI Bilim. Ve Tek. Dergisi-Journal Therm. Sci. Technol.* 35.1 (2015), pp. 1–9. ISSN: 1300-3615.

[33] V. G. Kourakos, P. Rambaud, S. Chabane, D. Pierrat, and J. M. Buchlin. “Two-phase flow modelling within expansion and contraction singularities”. In: *Comput. Methods Multiph. Flow V* 63 (2009), p. 27. ISSN: 1845641884. DOI: 10.2495/MPF090031.

[34] E. Deniz and N. Eskin. “Experimental and Numerical Investigation of Two-Phase Flow through Enlarging Singularity”. In: *Int. Refrig. Air Cond. Conf.* 2012, pp. 1–9.

[35] N. Eskin and E. Deniz. “Pressure drop of two-phase flow through horizontal channel with smooth expansion”. In: *Int. Refrig. Air Cond. Conf.* 2012, pp. 1–10.

[36] A. Ahmadpour, S. Noori Rahim Abadi, and R. Kouhikamali. “Numerical simulation of two-phase gas–liquid flow through gradual expansions/contractions”. In: *Int. J. Multiph. Flow* 79 (Mar. 2016), pp. 31–49. ISSN: 03019322. DOI: 10.1016/j.ijmultiphaseflow.2015.10.008.

[37] G. Ding, J. Chen, and Z. Li. “An investigation on the bubble breakup characteristics by recirculation flow in a venturi channel”. In: *Proceedings of the Fluids Engineering Division Summer Meeting*. Vol. Volume 3: Fluid Mechanics; Micro and Nano Fluid Dynamics; Multiphase Flow. Aug. 2021, V003T08A002. DOI: 10.1115/FEDSM2021-65716.

[38] M. Hundshagen, M. Mansour, D. Thévenin, and R. Skoda. “3D simulation of gas-laden liquid flows in centrifugal pumps and the assessment of two-fluid CFD methods”. In: *Exp. Comput. Multiph. Flow.* 3.3 (2021), pp. 186–207. DOI: 10.1007/s42757-020-0080-4.

[39] B.-D. Nguyen, S. Popp, M. Hundshagen, R. Skoda, M. Mansour, D. Thévenin, and C. Hasse. “Large eddy simulations of turbulent gas-liquid flows in a diverging horizontal channel using a hybrid multiphase approach”. In: *J. Fluids Eng.* 145.3 (Dec. 2022), p. 031501. ISSN: 0098-2202. DOI: 10.1115/1.4056209.

[40] M. Mansour. “Transport of two-phase air-water flows in radial centrifugal pumps”. PhD thesis. University of Magdeburg, Germany, 2020. DOI: 10.25673/32539.